Experiments in Fluids 36 (2004) 43–52
DOI 10.1007/s00348-003-0625-x

# Investigations on controlled transition development in a laminar separation bubble by means of LDA and PIV

**M. Lang, U. Rist, S. Wagner**



**Abstract** When a laminar boundary layer separates because of an adverse streamwise pressure gradient, the flow is subject to increased instability with respect to small-amplitude disturbances. Laminar–turbulent transition occurs under a rapid three-dimensional (3D) development within the separated shear layer. When the following turbulent boundary layer reattaches, a laminar separation bubble is formed. To allow controlled measurements, a small-amplitude Tollmien–Schlichting wave (TS wave) was introduced into the boundary layer without (case I) and with (case II) spanwise forcing of steady 3D disturbances. Combined application of laser-Doppler anemometry (LDA) and particle image velocimetry (PIV) demonstrates the suitability of both measurement techniques to capture the development of unsteady, periodic phenomena. The transition mechanism occurring in the flow field under consideration is discussed, and results obtained by controlled measurements are compared to direct numerical simulations (DNS) and predictions from linear stability theory (LST). Flow visualizations and stereoscopic PIV measurements give better insight into the 3D breakdown of the separated shear layer.

**Nomenclature**

| | |
|---|---|
| $a$ | amplitude |
| $f_0$ | fundamental frequency |
| $H_{12}$ | boundary layer shape factor, $H_{12}=\delta_1/\delta_2$ |
| $h$ | wavenumber coefficient in time |
| $k$ | wavenumber coefficient in the spanwise direction |
| $l$ | liter |
| $m$ | meter |
| $Re_x$ | Reynolds number based on streamwise distance of the leading edge |
| $Re_{\delta 1}$ | Reynolds number based on the displacement thickness $\delta_1$ |
| $s$ | second |
| $t$ | time |
| $u_\infty$ | freestream velocity |
| $u_\delta$ | velocity at the boundary layer edge |
| $u,v,w$ | velocities |
| $u',v'$ | velocity fluctuations |
| $x$ | streamwise coordinate |
| $y$ | wall-normal coordinate |
| $z$ | spanwise coordinate |
| $\delta$ | boundary layer thickness |
| $\delta_1$ | boundary layer displacement thickness |
| $\delta_2$ | boundary layer momentum thickness |
| $\lambda_z$ | spanwise wavelength |
| $\Phi$ | phase angle |

*Received: 15 October 2002 / Accepted: 4 March 2003*
*Published online: 12 July 2003*


M. Lang (✉), U. Rist, S. Wagner
Institut für Aerodynamik und Gasdynamik, Universität Stuttgart, Pfaffenwaldring 21, 70550 Stuttgart, Germany
E-mail: lang@iag.uni-stuttgart.de

## 1 Introduction

Laminar–turbulent transition is an important feature in aerospace aerodynamics because of its influence on fuel consumption via drag. Despite many years of research on fundamental mechanisms of the transition process in many generic configurations relevant to aircrafts, as well as other applications, there are situations that are less well understood and hence much more difficult to predict than certain 'standard' cases, as e.g. zero-pressure gradient flat-plate boundary layer transition.

The occurrence of boundary layer separation can essentially affect the efficiency of an entire system, for instance, the wing of a sailplane or even of a commercial aircraft. In the latter case, the Reynolds number for a slat is in the same range as for a wing of a sailplane. In addition to influencing drag, the occurrence of a laminar separation bubble causes noise. This is also an important aspect, e.g. in the consideration of wind-turbine blades.

Despite several fundamental experimental (Gaster 1966; Fitzgerald and Mueller 1988; Watmuff 1999) and numerical (Briley 1971; Spalart and Strelets 2000) investigations on transition in a laminar separation bubble, it is still difficult to predict and understand processes leading to the breakdown of the separated shear layer. The following experiments were carried out in a laminar water tunnel that was especially designed to study transition in boundary layers (Strunz and Speth 1987). Wiegand (1997) investigated transition in a Blasius boundary layer initiated by a point source using hot-film anemometry. Thereby, he also confirmed the high quality of the tunnel flow with a turbulence level of less than 0.05%. This low turbulence level in the free stream allows controlled investigations on amplification of intentionally excited small-amplitude disturbances in early stages of transition, which can be described by linear stability theory (LST) under the assumption of a parallel two-dimensional (2D) flow.

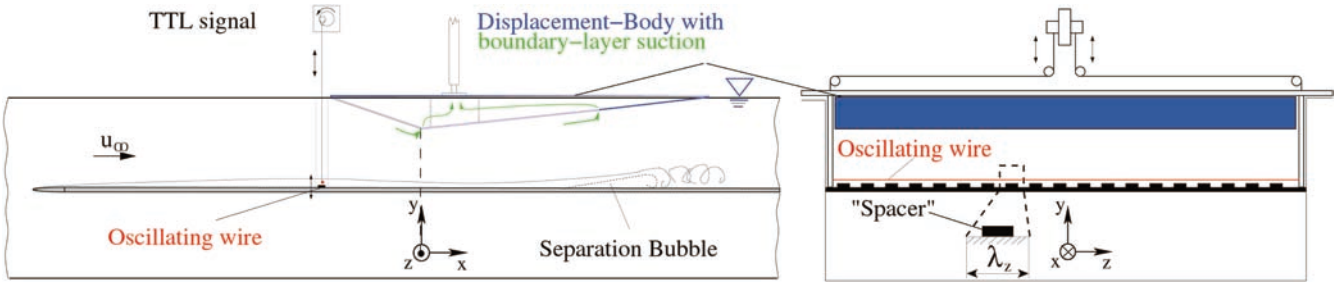




**Fig. 1.** Experimental setup in the test section of the laminar water tunnel

Because of large temporal and spatial scales in water, this facility is particularly suitable for highly resolved measurements in space and time and also for flow visualization. In addition, because of the sensitivity of the transition process, both applied nonintrusive measurement techniques (LDA and PIV) are suitable and reliable instruments for quantitative flow characterization. In this way, the presented method can measure unsteady, periodic 2D and three-dimensional (3D) phenomena by mono-PIV. This possibility led to a significant decrease in measuring time in comparison to LDA measurements.

## 2
## Experimental setup

A flat plate with an elliptical leading edge (axial ratio 10:1) was mounted in the test section of the laminar water tunnel. At the upper end of the flat plate a screen led to a pressure difference between the upper and the lower sides of the plate. Thus, fluid transport was forced through a gap between the plate and the tunnel side walls. This prevented the formation of an unstable corner boundary layer, thereby extending the streamwise range of laminar flow on the plate. At a free stream velocity of$u_\infty$=125 mm/s, a shape factor of $H_{12}$=2.6 was measured ($Re_x$=190,000, zero pressure gradient).

Since $H_{12}$ varied only about ±1% within a spanwise range of −200 mm ≤ $z$ ≤ 200 mm, a 2D flat-plate boundary layer can be assumed. To generate a pressure-induced laminar separation bubble, a displacement body was positioned in the test section above the flat plate (Fig. 1). After a short region of favorable pressure gradient, an adverse pressure gradient was applied. This is a common technique, which was also used by Gaster (1966). In the laminar water tunnel, a displacement body with a simple triangular shape was used. The cross-section ratio of 1:1.43 and an opening angle of 13° before and 5.1° after the narrowest section under the displacement body ($x$=0 mm) were ascertained by flow visualizations to achieve a laminar separation bubble with reasonable size for high-resolution measurements.

Boundary layer suction was applied at the displacement body at the narrowest section and through another suction strip in the region of adverse pressure gradient ($x$=305 mm). This prevented separation and transition on the displacement body itself. The necessary suction rate (0.483 l/(s m)) was established by flow visualizations.

The experiment was performed under controlled conditions to suppress low-frequency background disturbances (such as flapping, Boiko et al. 2002) which occur under natural (undisturbed) conditions. Therefore, a small-amplitude 2D Tollmien–Schlichting wave (TS wave) was forced by an oscillating wire. The wire was positioned in the critical layer in the region of favorable pressure gradient ($x$=−230 mm). The power unit of the disturbance source generated a TTL trigger signal each period, which was taken as time reference for phase-locked measurements. To stay close to the natural case, the disturbance amplitude was very weak compared to other investigations ( Alam and Sandham 2000). The fundamental frequency $f_0$=1.1 Hz was chosen to match the most-amplified frequency according to linear stability theory. In the undisturbed (natural) case, vortex shedding occurs with the same frequency, but with varying amplitudes in time (flapping) when compared to the case with disturbance input. Further investigations on the influence of initial disturbance levels are given in Boiko et al. (2002) and Rist (2002) so that the amplitude in the present case was fixed.

## 3
## Data acquisition and analysis

In order to introduce a 3D disturbance, thin (1.0 mm) metal plates were placed regularly underneath the oscillating wire. These so-called ‘spacers’ cause a steady 3D disturbance mode that interacts with the TS wave. This results in a 3D wave combination with typical peak–valley structure (Fig. 2) where the boundary layer is thicker in the peak plane compared to the valley plane (Klebanoff et al. 1962; Kruse and Wagner 1996; Kruse 1997). An advantage of 3D disturbance input is that vortex structures, appearing with the onset of transition, are fixed in the spanwise direction. In the present measurements with 3D disturbance input, the spanwise wavelength was set to $\lambda_z$=58 mm, so that regularly appearing spanwise vortex structures could be seen in the transition region. Flow visualizations using the hydrogen bubble technique were carried out to determine the spanwise wavelength (Fig. 3).

A two-component LDA (Dantec, Denmark) was used to measure the velocity components $u(t)$ in the downstream direction and $v(t)$ perpendicular to the flat plate (Kruse and Wagner 1996). In contrast to hot-film anemometry, the ability of LDA to identify velocities with their value and direction is an important benefit in the transition region of the separated shear layer with its strong bidirectional velocity fluctuations. Thus, the dividing streamline can be determined directly from the measured velocity profiles.

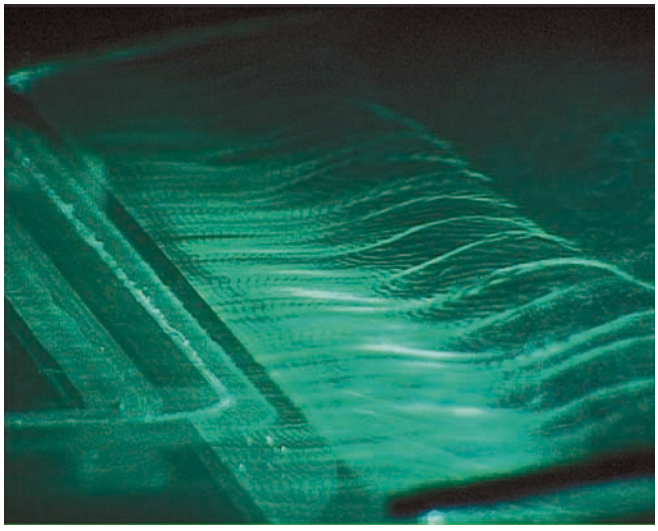

**Fig. 2.** 3D disturbance wave combination with spanwise modulation caused by spacers. Visualization of the separated shear layer with hydrogen bubbles (*perspective view*)

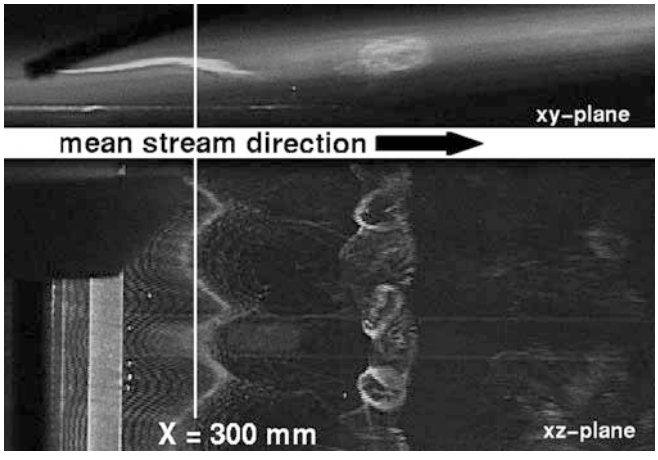


**Fig. 3.** Shear layer roll-up with 3D vortex shedding in the transition region of the laminar separation bubble

The PIV system was a DLR system (Deutsches Zentrum für Luft-und Raumfahrt, Germany) and was expanded to stereoscopic PIV (SPIV). It consisted of a double-pulsed Nd:YAG laser (Quantel Twins, 2×150 mJ) two CCD cameras (PCO Sensicam, 1280 pixel ×1024 pixel) and an external sequencer (DLR). The good optical access to the test section from three sides allowed PIV and SPIV measurements in all Cartesian planes of the flow field. To minimize optical distortions (e.g. astigmatism) caused by diffraction in water, the optical axis of a camera must be aligned almost perpendicular to the border of the two optical media. Therefore, in the case of SPIV measurements, water-filled prisms (Westerweel and van Oord 2000) or tanks with mirrors were mounted at the tunnel sidewalls to allow different viewing angles of up to ±45° to the measurement volume.

LDA measurements were performed starting from the beginning of adverse pressure gradient ($x$=0 mm) until shortly beyond the onset of disturbance saturation ($x \approx 310$ mm). The resolution of the flow field in streamwise direction in the transition region was $\Delta x$=10 mm. In the case of 3D disturbance input, the spanwise wavelength was sampled with 16 boundary layer profiles in the spanwise direction. A wall-normal step size of $\Delta y$=1 mm provided a resolution of boundary layer profiles with about 25–30 points depending on the local boundary layer thickness. The record length of all measured points was 30 fundamental disturbance periods (wire cycles). For an exact determination of amplitudes and phases of the fundamental frequency an its higher harmonics, a phase-averaging technique with respect to the TTL signal of the disturbance source was applied.

Because of the long measurement times with the LDA in water, small structures cannot be sufficiently resolved. Here the PIV (SPIV) with its high spatial resolution provides better results concerning the detection of structures in the transition region. Additionally, the third velocity component $w$ can be measured, which is not accessible with the two-component LDA. The recorded PIV datasets were dewarped (in the case of SPIV) and evaluated with a FFT-based cross-correlation method. A Levenberg–Marquardt peak-fitting algorithm provided subpixel accuracy and minimized peak-locking effects (Ronneberger et al. 1998). Spurious vectors (in general, less than 2–5%) were deleted and reinterpolated by a fit to their neighbors.

In the case of amplitude measurements by PIV, the field of view was about 58×50 mm$^2$. With a sampling window size of 32 pixel×32 pixel and a 16-pixel step size, the resolution of the wall-normal boundary layer profiles occurred with 40–50 points and was consequently higher than that obtained by LDA measurements. To capture the fundamental frequency, with its higher harmonics in the case of a 2D disturbance input, phase-locked measurements with respect to the disturbance source were carried out for one $x$–$y$-plane (an average of 30 disturbance periods). The phase angle was shifted regularly over 18 time-steps to sample the fundamental period. Because of the necessary spatial resolution in the case of 3D disturbance input, the flow field was additionally scanned with the laser light-sheet over one spanwise wavelength $\lambda_z$. For this, the light-sheet optics and the camera were mounted on two different traverses to move independently in the spanwise $z$-direction. Thus, the camera movement could be corrected (because of diffraction into water) to keep the focus in the light-sheet plane. Furthermore, it was important to achieve exactly the same field of view for each spanwise position. The traverses were coupled with the PIV system by custom acquisition software. Therefore, data acquisition could be completely automated to record phase-locked data sets with spanwise resolution. According to LDA measurements, the step size in the span was set to 16 positions over one spacer wavelength $\lambda_z$.

In order to obtain temporal and spanwise wavenumbers in the case of 3D disturbance input, a double Fourier transform in time and the spanwise direction was applied according to the following approach (Kruse 1997; Lang et al. 2000a):

$$u'(x,y,z,t) = \sum_{h=1}^{H} a_h(x,y,z)\sin[h2\pi f_0 t + \phi_h(x,y,z)],$$

$$= \sum_{h=1}^{H}\sum_{k=-K}^{K} a_{h,k}(x,y)\sin\left[h2\pi f_0 t - k\frac{2\pi}{\lambda_z}z + \phi_{h,k}(x,y)\right].$$

This yielded the amplitudes $a_{h,k}$ and phases $\Phi_{h,k}$ of the measured disturbance wave-combination. The indices $h$ and $k$ denote the wavenumber coefficients in time and the spanwise direction, respectively. This phase-averaging technique can be used until small-scale and strong non-periodic 3D structures occur downstream of disturbance saturation in the reattachment region of the laminar separation bubble.



## 4 Results

In the present results the Reynolds number based on the displacement thickness at the separation line is $Re_{\delta 1}$=900. The extent of the laminar separation bubble of about 270 mm is given by the mean dividing streamline (DSL, Fig. 4) with the net mass flux set to zero (Fitzgerald and Mueller 1988)

$$\int_{y=0}^{y_{DSL}} \bar{u}(y)\mathrm{d}y = 0.$$

The first section of the laminar separation bubble is dominated by a primary convective instability of the 2D TS wave (Maucher et al. 1999). Therefore, the development of this fundamental mode was examined in detail. Two cases were considered.

In case I, the introduced disturbance was 2D (TS wave, oscillating wire without spanwise modulation by spacers). Results from phase-locked PIV measurements are compared to appropriate LDA data and LST.

In case II, a 3D disturbance was enforced by the oscillating wire in combination with spacers as described in Sect. 2. These spacers caused steady 3D disturbances, which generated unsteady 3D disturbance modes (oblique traveling waves) together with the TS wave (2D time harmonic). Thus, the 2D time harmonics were also included in case II. Results for time-averaged and unsteady quantities from LDA measurements are compared to LST and 3D-DNS (Marxen et al. 2002). Further, amplitude and phase distributions as well as the amplification of dominant disturbance modes from spanwise resolved, phase-locked PIV measurements are compared to LDA results and LST.

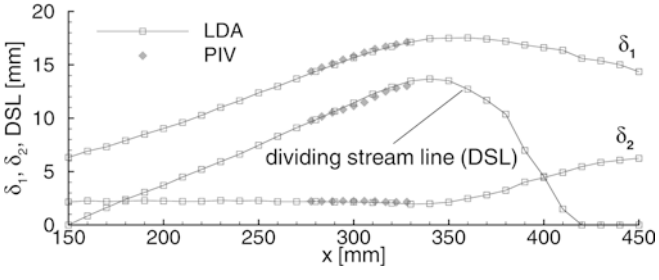


**Fig. 4.** Mean boundary layer quantities measured by PIV in comparison with LDA data

### 4.1 Case I, 2D disturbance input

A detailed comparison of boundary layer quantities from LDA measurements, linear stability theory (LST) and direct numerical simulations (DNS) under consideration of a 2D disturbance input was presented in Lang et al. (2000a, 2002b). Very good agreements were obtained for base flow variables as well as for unsteady quantities. Now, additional PIV measurements were performed in the region of linear amplification (according to LST) until beyond the onset of disturbance saturation. To capture unsteady phenomena, phase-locked measurements were carried out in one $x$–$y$-plane. Averaging the whole data set (with 18 steps in time) over one fundamental period yielded mean boundary layer quantities. Figure 4 shows a very good agreement of the displacement thickness $\delta_1$, momentum thickness $\delta_2$ and the dividing streamline in the saturation region, obtained from PIV data in comparison with LDA measurements. Because of the limited field of view with the PIV technique, the measurement position was chosen to be in the region of disturbance saturation were transition occurs.

It can be shown that the accuracy of PIV is sufficient not only to measure instantaneous field data. It is also a suitable instrument to measure small-amplitude periodic phenomena (of less than <5% of the boundary layer edge-velocity $u_\delta$). A Fourier analysis of 18 phase-averaged instantaneous boundary layer profiles, with the phase angle regularly shifted over one fundamental period as mentioned before, yielded wall-normal amplitude distributions of the fundamental frequency (TS wave) and its higher harmonics. For validation, a comparison with corresponding phase-averaged LDA measurements of wall-normal amplitude distributions are given in Fig. 5 for three streamwise positions in the region of linear amplification (according to LST). Figure 6 shows the amplification of the shear layer maximum $u'_{max}(x)$ obtained from PIV data in comparison with the amplification rate

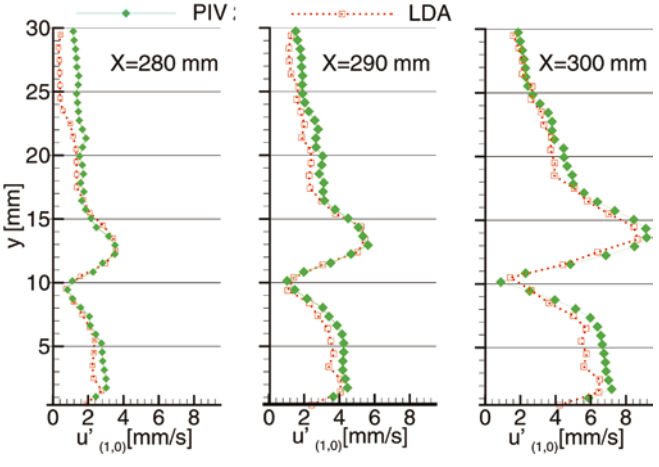


**Fig. 5.** Amplitude distributions $u'(y)$ of the (1,0) mode. PIV results in comparison with corresponding LDA measurements in the region of linear (LST) amplification

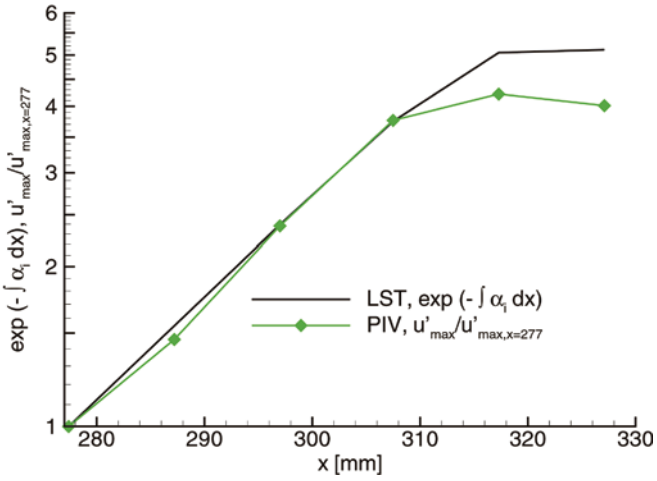


**Fig. 6.** Amplification of the shear layer maximum $\left(\frac{u'_{max}(x)}{u'_{max}(x=277\text{ mm})}\right)$, (1,0) mode measured by PIV compared to results of LST in the region of linear amplification until beyond disturbance saturation

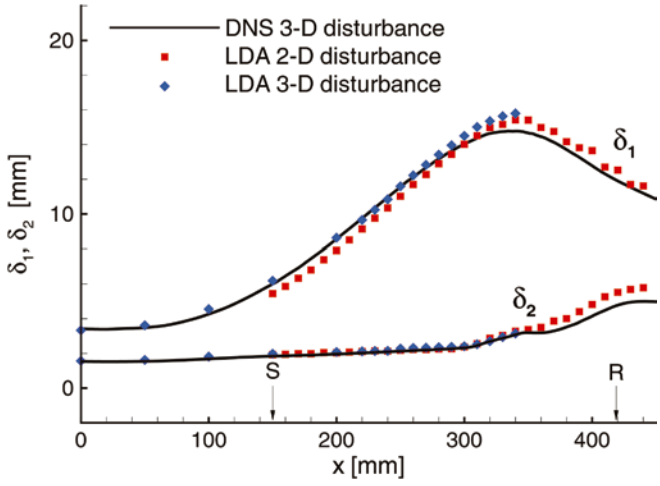


**Fig. 7.** Comparison of boundary layer mean quantities over the whole separated region (*SR*) with 2D and 3D disturbance input. *S*, separation point; *R*, reattachment region

predicted by LST (normalized by $u'_{max}(x=277\text{ mm})$). The amplification curve of this disturbance mode matches theory very well until the onset of saturation downstream $x$=310 mm. Here, a rapid nonlinear 3D development starts, leading to the 3D breakdown of the separated shear layer, which cannot be described by LST.

The possibility of measuring unsteady phenomena by means of PIV has one important benefit. Measuring time in the linear and weakly nonlinear regions of amplification can be decreased by more than a factor of 10 in comparison to LDA measurements.

## 4.2 Case II, 3D disturbance input

### 4.2.1 Comparison of LDA measurements with LST and DNS

General properties are first discussed using base flow variables obtained from LDA data in comparison with DNS. Here, base flow means quantities averaged in time and in the spanwise direction. Note that the laminar separation bubble is a highly unsteady phenomenon, and the base flow can never be observed instantaneously at any time step. Therefore the time- and space-resolved disturbance quantities must also be considered before claiming that the same physics are captured in the experimental and numerical investigations. In the available DNS data, the disturbance input was realized by suction and blowing at a position after the onset of adverse pressure gradient (Fig. 8). The TS amplitude was chosen in a way to match the experimental results (Marxen et al. 2002).

In Fig. 7 boundary layer quantities measured by LDA are shown for both cases of disturbance input (2D and 3D) in comparison with DNS. The boundary layer displacement thickness $\delta_1$ increases considerably along the separation bubble, while the momentum thickness $\delta_2$ does not start to increase until the onset of transition. Good agreement between DNS results and measurements reveals that a separation bubble of approximately the same size was formed in both cases. As can be seen in Fig. 7, the boundary layer parameters over the separated region are nearly the same for 2D and 3D disturbance input. The same holds true for the size of the bubble. Similar results can be also seen from the investigations of Rist et al. (2000). This confirms that the development of the 2D TS wave is decisive for the transition process in the considered case, and the disturbed steady 3D mode (caused by spacers) does not play an important role. Therefore, in the case of 3D disturbance input, the development of 2D time-harmonic quantities were examined in detail.

Figure 8 shows the amplification of the maximum amplitude $u'_{max}(x)$ within the wall-normal amplitude distributions normalized with the edge-velocity of the boundary layer profile in the narrowest section ($u_\delta(x=0\text{ mm})=174$ mm/s). It can be seen that the fundamental mode ((1,0), TS wave) is strongly amplified in the region of the separated shear layer. Experimental and numerical results match perfectly from $x$=230 mm onwards, even shortly beyond saturation. Good agreement with LST confirms the primary convective nature of the

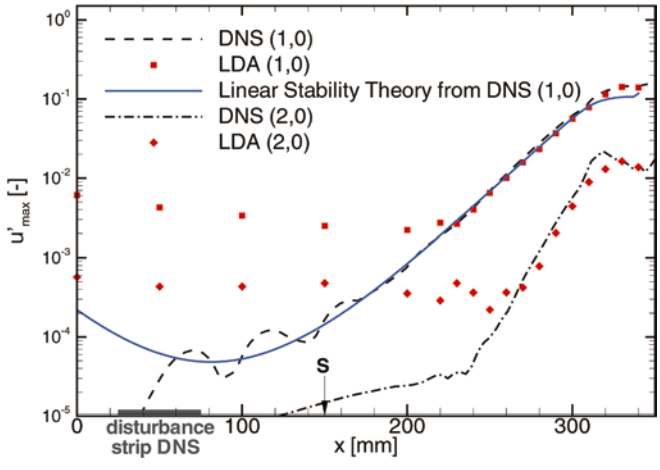


**Fig. 8.** Amplification of 2D time harmonics (*h*,0 modes, TS wave) with 3D disturbance input. *S*, separation point

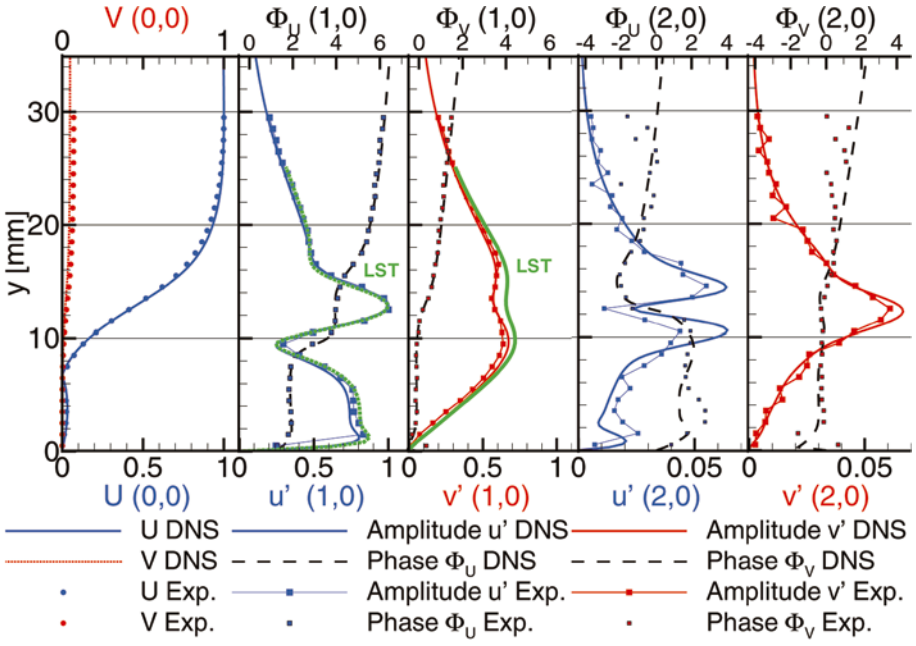


**Fig. 9.** Mean boundary layer profiles ($u$ and $v$, (0,0) mode) with wall-normal amplitude and phase distributions of the 2D time harmonics measured by LDA compared to DNS and LST for streamwise position $x$=290 mm

disturbance. As can be seen from Fig. 8, DNS and the experiments also predict the same amplitudes, growth rate and saturation level for the nonlinearly generated higher harmonic disturbance (2,0). Both disturbances saturate at the position of shear layer roll-up around $x$=310 mm.

Wall-normal amplitude and phase distributions for the $u$ and $v$ components are compared to LST and DNS in Fig. 9 at a location near the center of the measurable region of linear amplification ($x$=290 mm, normalized by $u'_{max}(x=290\ mm)$ of the fundamental mode). The detached shear layer corresponds to the location of the inflection point within the $u$-velocity profile around $y$=13 mm.

At this stage the TS wave exhibits an amplitude maximum in the detached shear layer that resembles the eigenfunction of a Kelvin–Helmholtz instability. But, as can be seen by a further maximum in the near-wall region, the influence of damping viscid effects may not be neglected. The measured amplitude distributions of these 2D time harmonics perfectly match DNS results, even for the first higher harmonic (2,0 mode).

In the experiment, a strong initial steady disturbance with half the spacer wavelength (0,2 mode) can be observed (Fig. 10) that cannot be modeled in the DNS so far. From good agreement with LST for the development of the fundamental mode, it can be concluded that the spanwise modulation of the base flow does not exert any influence on 2D instability characteristics of the flow field. In contrast, the growth of spanwise modulated perturbations of fundamental frequency (1,±2 modes) is decisively affected by the presence of this steady mode. The growth rate of these disturbances cannot be explained by linear theory, or by a secondary convective (Rist 1998) or temporal (Maucher et al. 1999) instability, since it already sets in well before the TS wave has gained sufficiently large amplitude. Instead, nonlinear interaction between the TS wave (1,0 mode) and the large steady disturbance (0,2) generates modes (1,±2) with approximately the same amplification

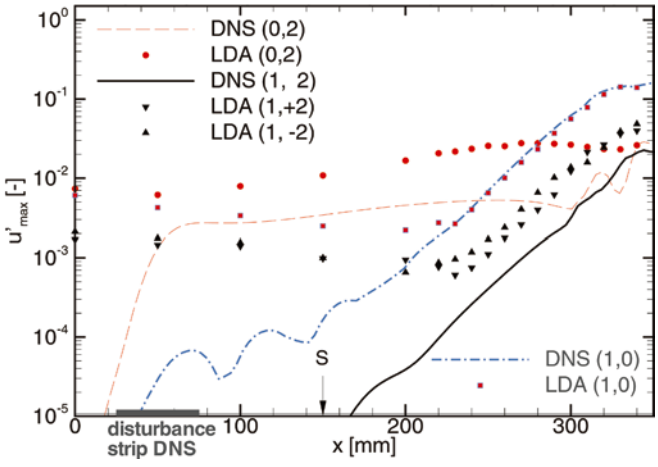


**Fig. 10.** Amplification of steady and unsteady 3D disturbance modes in comparison with (1,0) mode from LDA and DNS data. *S*, separation point

rate as mode (1,0). Results from a spanwise-symmetrical DNS confirm this fact by showing the same growth rate for mode (1,2) only in the presence of a large steady disturbance mode (0,2). Agreement of amplitude and phase distributions between experiment and DNS is reasonable (Fig. 11) albeit some deviations from symmetry can be seen in the measurements (Fig. 10) that are not considered in the DNS.

Characteristics of the separation bubble have proven to be the same in a DNS with and without forced steady 3D disturbances (Marxen et al. 2002). The same holds for the experiment with and without spacers (Fig. 7) suggesting that the large initial disturbance level of steady 3D disturbances plays only a minor role in this transition process. Instead, the dominating mechanism at work seems to be an absolute secondary instability of 3D disturbances as identified by Maucher et al. (1999) which is independent of the level of incoming 3D dis-

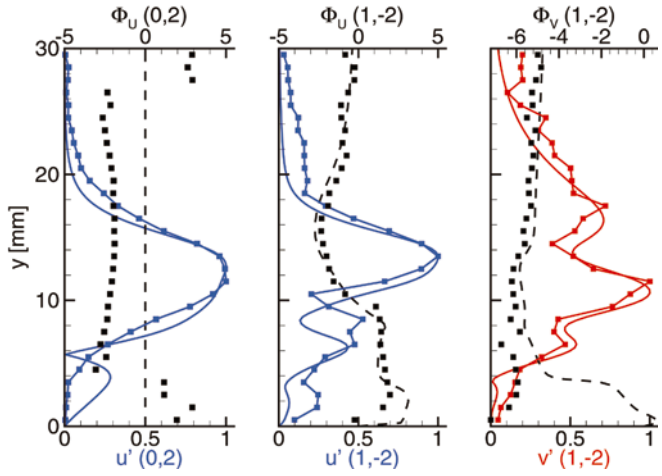


**Fig. 11.** Wall-normal amplitude and phase distributions of one steady (0,2) and unsteady ((1,-2) oblique wave) disturbance mode normalized with their maximum amplitude for streamwise position $x$=290 mm

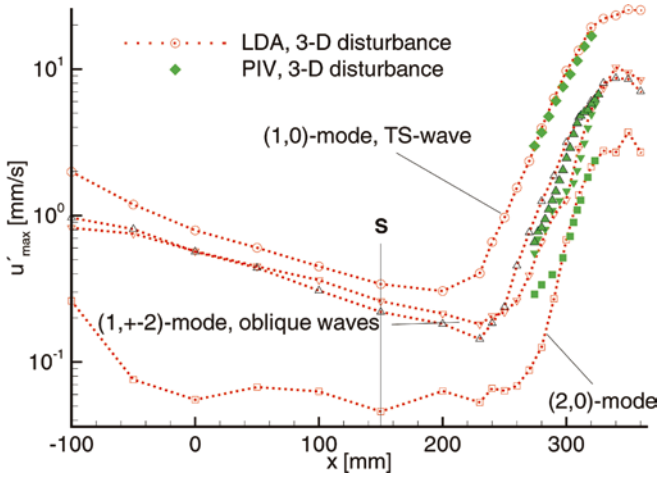


**Fig. 13.** Amplification $u'_{max}(x)$ of unsteady 2D and 3D (oblique waves) disturbance modes measured by spanwise resolved mono-PIV in comparison with LDA data.*S*, separation point

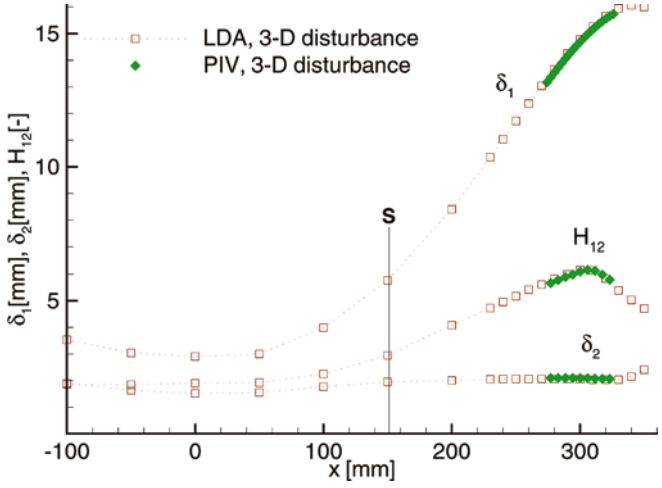


**Fig. 12.** Mean boundary layer quantities obtained by spanwise resolved mono-PIV measurements compared to LDA data (3D disturbance input). *S*, separation point

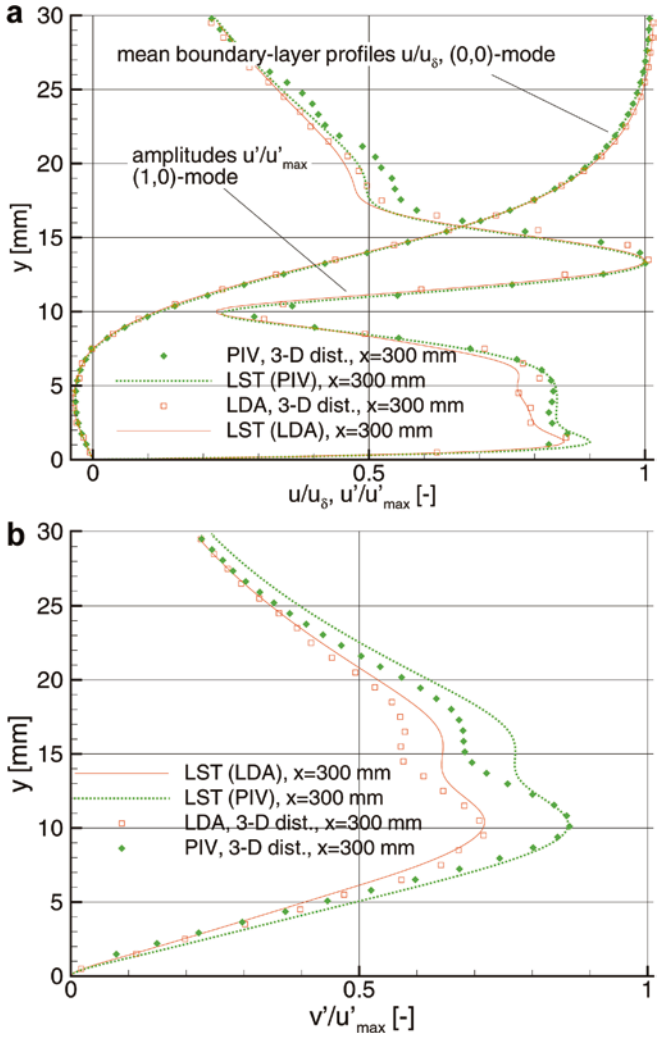


**Fig. 14.** Mean boundary layer profiles for the velocity component $u$ (**a**) and wall-normal amplitude distributions for both measured velocity components $u$ (**a**) and $v$ (**b**) from LDA and PIV measurements compared to LST ($x$=300 mm, 3D disturbance input)

turbances (Marxen et al. 2003). Hence, differences in amplitude and amplification of DNS and experiment for the mode (0,2) are not critical.

### 4.2.2
### Comparison of PIV measurements with LDA and LST

In the region of linear disturbance amplification, mono-PIV measurements ($x$–$y$-plane) were carried out to measure the development of the input 3D disturbance wave combination. Eighteen phase-locked measurements shifted ($\Delta\Phi$=20°) over one fundamental period (TS wave) in time and one spacer wavelength $\lambda_z$ in the spanwise direction provided phase-averaged PIV data of instantaneous boundary layer profiles as described in Sect. 3. The results of the double Fourier transform applied to this PIV data set agree very well with corresponding spanwise-resolved LDA measurements.

In Fig. 12 mean boundary layer quantities computed from LDA and PIV data are compared. For this, the boundary layer profiles were averaged in time and span (0,0 mode). Excellent agreement is achieved for mean quantities as well as for the amplification of velocity fluctuations $u'_{max}(x)$ shown in Fig. 13. The selected $(h,k)$ modes in Fig. 13 are dominant for the transition process in the considered case and have been compared to DNS before. The very good agreement of unsteady disturbance development obtained from both measurement techniques justifies the use of mono-PIV for measurements of small-amplitude (periodic) phenomena. By applying the PIV technique with spatial resolution instead of LDA, a significant decrease in measurement time can also be achieved in the case of 3D disturbance input.

In Fig. 14, mean boundary layer profiles for the velocity component $u$ together with their wall-normal amplitude distributions for the fundamental mode (1,0) obtained by the double Fourier transform, are compared to LST at a single streamwise position ($x$=300 mm) just before the onset of disturbance saturation. Additionally, a comparison for the second measured velocity component $v$ is also shown in Fig. 14. The deviations in amplitude distributions of the two separate measurements (LDA–PIV) are due to a slight difference in the base flow, as can be seen in the region of the boundary layer edge around $u/u_\delta$=1. The reason for this deviation of about 1% $u_\delta$ at this position is the reproducibility in the case of a completely new experimental setup. However, the very good agreement with predictions of LST proves that the velocities and their fluctuations are accurately determined from both data sets, even in the region of strong velocity gradients within the shear layer. The results of LST are based on the measured mean velocity profile $u(y)$ (averaged in time and span, Fig. 14), which must be determined very accurately because its second derivative plays an important role according to the Orr–Sommerfeld equation.

In Fig. 15 wall-normal amplitude ($u'(y)$ and$v'(y)$) and phase distributions ($\Phi_u(y)$ and$\Phi_v(y)$) for the disturbance modes illustrated in Fig. 13are compared. It is at the same streamwise position ($x$=300 mm) as already compared to LST in Fig. 14. It can be seen that even the higher harmonics ($u'_{(2,0)}$,$v'_{(2,0)}$) could be accurately measured by PIV, although their amplitude is less than 1% of the boundary layer's edge velocity $u_\delta$ at this position. The constant offset in phase distributions means a change in phase velocity, which is an effect of the slight deviation in the base flow, as mentioned above.

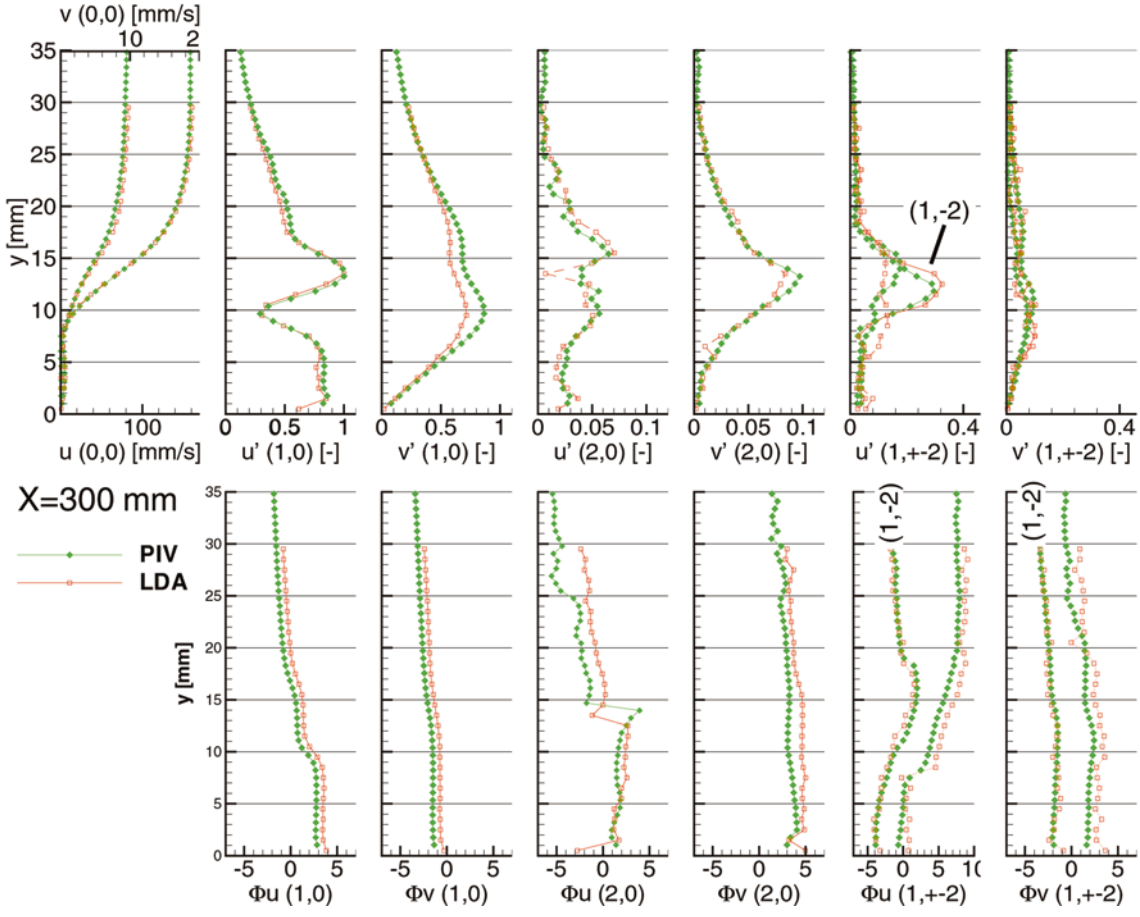


**Fig. 15.** Wall-normal amplitude and phase distributions (2D time harmonics and oblique waves) from spanwise resolved PIV measurements compared to LDA data for velocities $u$ and$v$ ($x$=300 mm, 3D disturbance input)

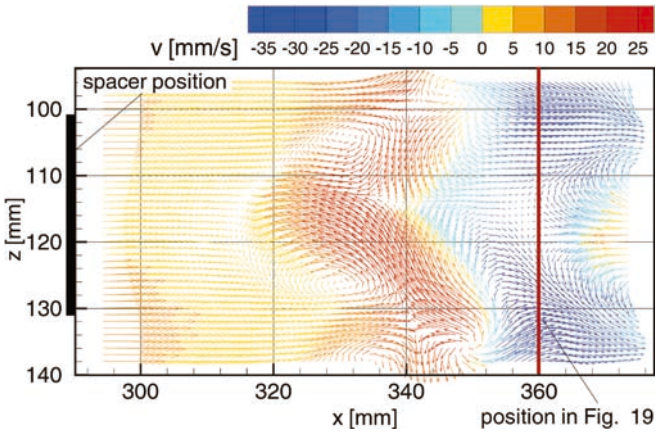


**Fig. 16.** 3D breakdown of the separated shear layer with counter-rotating vortex pairs. Results from phase-locked stereoscopic PIV measurements in the *x*–*z*-plane (*y*=16 mm, average of 25 measurements). *Red bar*, *x*-position in Fig. 18

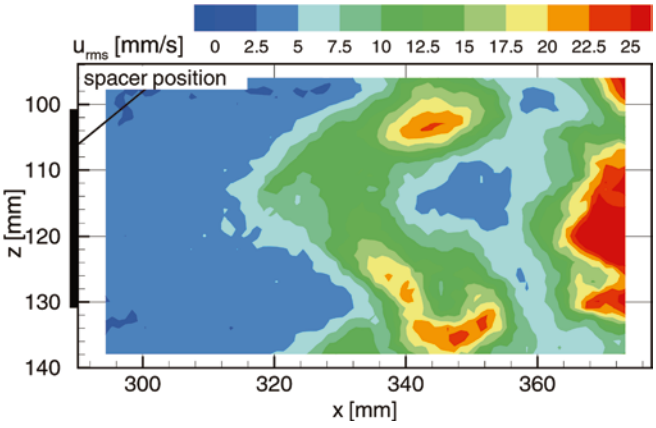


**Fig. 17.** RMS values for velocity component *u* obtained by averaging 25 measurements. First nonperiodicities in the regions of vortex pairs (high rms values)

### 4.2.3
### Results from stereoscopic PIV measurements

Despite a complicated setup at the water tunnel because of diffraction effects between two optically different media, application of SPIV is superior to a monosystem for the detection of transitional structures, as can be seen in the following results. In the transition region with its strong 3D development and bidirectional fluctuations, the possibility to capture all three velocity components simultaneously gives an additional insight into the 3D breakdown of the separated shear layer. Figure 16 shows the average of 25 phase-locked SPIV measurements with the light sheet aligned parallel to the flat plate (*y*=16 mm). Contour colors denote the out-of-plane component *v*. A rapid 3D breakdown of the separated shear layer downstream the onset of saturation (*x*=310 mm) under the occurrence of counter-rotating vortex pairs is as clearly visible as the dominance of the TS wave, responsible for the strong vortex shedding in the transition region (Figs. 2 and 19, *x*–*y*-plane). In the vicinity of these counter-rotating vortices, fluid is moved from inside the separation bubble up into the separated shear layer (yellow and red contour colors, Fig. 16) leading to the 3D breakdown. Because of strong velocity gradients in this region, first nonperiodicities occur in the flow field, which means high rms values when multiple measurements are averaged, as can be seen in Fig. 17 for the velocity component *u*.

Figure 18 shows the average of 25 SPIV measurements in the *y*–*z*-plane (perpendicular to the mean flow) at a streamwise position*x*=360 mm (red bar in Fig. 16). The measurements were taken phase-locked at an equal phase angle to the measurement shown in Fig. 16. Again, the out-of-plane component perpendicular to the light-sheet plane is denoted by colors (here velocity component *u*). In the vicinity of counter-rotating vortex pairs a strong back flow can be detected (blue colors). In Fig. 19 such a vortex pair can be seen from flow visualization (red ellipse). Here, fluid within the LSB (isolated by the dividing streamline) is blue-colored, and one layer is additionally marked with a carpet of hydrogen bubbles

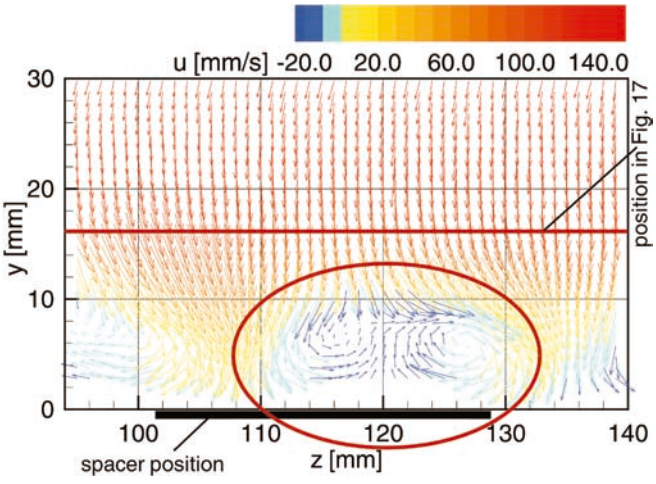


**Fig. 18.** Results from stereoscopic PIV measurements in the *y*–*z*-plane (*x*=360 mm). Counter-rotating vortex pairs in the transition region of the laminar separation bubble with strong back flow. *Red bar*, *y*-position in Fig. 16

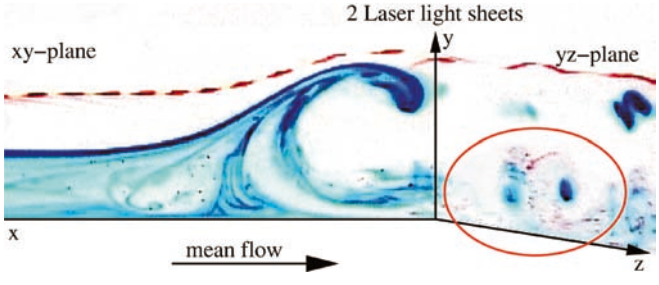


**Fig. 19.** Vortex shedding in the transition region. Visualization with two perpendicular aligned laser light-sheets (*x*–*z*- and *y*–*z*-plane, *perspective view*).*Blue*, fluid enclosed by the dividing streamline (instantaneous view); *red lines*, hydrogen-bubble carpet as can be seen in Figs. 2 and 3

(red). For this picture two laser light-sheets were aligned in the streamwise direction (*x*–*y*-plane) and perpendicular to the mean flow (*y*–*z*-plane) respectively. In the *x*–*y*-plane

the roll-up of the separated shear layer can be seen, while the $y$–$z$-plane shows the spanwise deformation with 3D vortex structures in the transition region.

## 5 Conclusions

A detailed investigation on controlled transition in a laminar separation bubble was performed. The onset of 3D vortex structures causing the breakdown to turbulence of a separated boundary layer was measured and visualized using phase-averaged LDA, phase-locked PIV and stereoscopic PIV. A method to measure small-amplitude unsteady phenomena of 2D and 3D disturbance modes by PIV was shown. Comparisons with corresponding LDA measurements and linear stability theory exhibit very good agreement. The possibility to measure unsteady phenomena using PIV has led to a significant decrease in measurement time compared to adequate LDA measurements.



The experimental results were also compared to direct numerical simulations. The velocity field of the transitional separation bubble showed very good agreement for time-averaged and unsteady quantities. Transition in a separation bubble is driven by a convective primary amplification of the 2D TS wave, mainly determining the size and position of the bubble. The initial level of steady 3D disturbances in the inflow plays a minor role in the considered transition process. This was clearly identified from the existing data.

Stereoscopic PIV measurements gave a new and closer insight into the 3D development of the transitional shear layer. In the transition region with its strong bidirectional fluctuations vortex structures leading to 3D breakdown were measured. These structures were up to now only accessible by qualitative flow visualizations or mono-PIV.

## References


Alam M, Sandham ND (2000) Direct numerical simulation of 'short' laminar separation bubbles with turbulent reattachment. J Fluid Mech 410:1–28

Boiko AV, Grek GR, Dovgal AV, Koslov VV (2002) The origin of turbulance in near-wall flows. Springer, Berlin Heidelberg New York

Briley WR (1971) A numerical study of laminar separation bubbles using the Navier–Stokes equations. J Fluid Mech 47:713–736

Fitzgerald EJ, Mueller TJ (1988) Measurements in a separation bubble on an airfoil using laser velocimetry. AIAA J 28:584–592

Gaster M (1966) The structure and behavior of laminar separation bubbles. AGARD CP 4:813–854

Klebanoff PS, Tidstrom KD, Sargent LM (1962) The three-dimensional nature of boundary layer instability. J Fluid Mech 12:1–41

Kruse M, Wagner S (1996) Measurements of laminar–turbulent transition in a flat-plate boundary layer. In: Proceedings of the 8th international symposium of laser techniques to fluid mechanics, Lisbon, 8–11 July

Kruse M (1997) Einsatz der Laser-Doppler-Anemometrie zur Untersuchung des laminar-turbulenten Grenzschichtumschlags an der ebenen Platte. Dissertation, University of Stuttgart, Germany

Lang M, Marxen O, Rist U, Wagner S (2000a) Experimental and numerical investigations on transition in a laminar separation bubble. In: Wagner S et al. (eds) Notes on numerical fluid mechanics, new results in numerical and experimental fluid mechanics. Springer, Berlin Heidelberg New York

Lang M, Marxen O, Rist U, Wagner S (2000b) LDA-Messungen zur Transition in einer laminaren Ablöseblase. In: Proceedings of 8th Fachtagung der GALA, Lasermethoden in der Strömungsmesstechnik, Freising-Weihenstephan, Germany, 12–14 Sept. Shaker, Aachen

Marxen O, Lang M, Rist U, Wagner S (2002) A combined experimental/numerical study of unsteady phenomena in a laminar separation bubble. In: Proceedings of IUTAM symposium "unsteady separated" flows, Toulouse (available on CD-ROM)

Marxen O, Rist U, Wagner S (2003) The effect of spanwise-modulated disturbances on transition in a 2-D separated boundary layer. AIAA paper no. 2003-0789

Maucher U, Rist U, Wagner S (1999) Transitional structures in a laminar separation bubble. In: Nitsche W, Heinemann R, Hilbig HJ (eds.) Notes on numerical fluid mechanics, new results in numerical and experimental fluid mechanics. Vieweg, Wiesbaden

Rist U (2002) On instability and transition in laminar separation bubbles. In: Proceedings of CEAS aerospace aerodynamics research conference, Cambridge, UK, 10–12 June 2002, (available on CD-ROM)

Rist U (1998) Zur Instabilität und Transition in laminaren Ablöseblasen. Habilitation, Universität Stuttgart, Shaker, Aachen

Rist U, Augustin K, Wagner S (2000) Numerical simulation of laminar separation-bubble control. In: Wagner S et al. (eds) Notes on numerical fluid mechanics, new results in numerical and experimental fluid mechanics. Springer, Berlin Heidelberg New York

Ronneberger O, Raffel M, Kompenhans J (1998) Advanced evaluation algorithms for standard and dual plane particle image velocimetry. In: Proceedings of 9th international symposium of laser techniques to fluid mechanics, Lisbon, 13–16 July

Spalart PR, Strelets MK (2000) Mechanisms of transition and heat transfer in a separation bubble. J Fluid Mech 403:329–349

Strunz M, Speth JF (1987) A new laminar water-tunnel to study the transition process in a Blasius boundary layer and in a separation bubble and a new tool for industrial aerodynamics and hydrodynamic research. AGARD CP 413:25-1– 25-5

Watmuff J (1999) Evolution of a wave packet into vortex loops in a laminar separation bubble. J Fluid Mech 397:119–169

Westerweel J, van Oord J (2000) Stereoscopic PIV measurements in a turbulent boundary layer. In: Stanislas M, Kompenhans J, Westerweel J (eds) Particle image velocimetry, progress toward industrial application. Kluwer, Dordrecht

Wiegand T (1997) Experimentelle Untersuchungen zum laminar-turbulenten Transitionsprozess eines Wellenzuges in einer Plattengrenzschicht. Dissertation, University of Stuttgart, Germany